Hindawi
International Journal of Aerospace Engineering
Volume 2022, Article ID 2414019, 13 pages
https://doi.org/10.1155/2022/2414019

Research Article

Analyses of the Design of Multirows Vaneless Staggered Counter-Rotating Turbine

Zhongye Wu, Yukun Zhang, Qingfen Ma, and Jingru Li

School of Electromechanical Engineering, Hainan University, Hainan 570228, China

Correspondence should be addressed to Zhongye Wu; wuzhongye@126.com

Received 13 June 2022; Revised 1 December 2022; Accepted 1 December 2022; Published 28 December 2022

Academic Editor: Jiaying Zhang

Compared with a conventional turbine, counter rotating turbine has larger thrust weight ratio, shorter axial distance, and higher efficiency. It has been widely used in high-performance aviation. In conventional counter-rotating turbine, HPT is located in the front of LPT, and only a stator row can be eliminated. The layout limits the turbine weight and efficiency. Therefore, the staggered counter rotating turbine is proposed, and the staggered counter rotating turbine can eliminate the all-internal stators, which can greatly improve the turbine weight and efficiency. The staggered counter rotating turbine is the development and improvement of counter rotating turbine. Due to the elimination of the all-internal stators, the downstream rotor will suffer from the insufficient inlet swirl, which is the main question in staggered counter rotating turbine design. Furthermore, the turbine outlet angle is also an important parameter to evaluate the turbine design. The coordination of inlet swirl and outlet Mach number and the outlet angle is discussed by the theoretical method. In order to verify the design method, two-dimensional throughflow design, blade design, and three-dimensional numerical analysis are performed. Expansion ratios and efficiency at the speed combinations of the 80% to 105% are discussed to reveal the turbine characteristics at off-design conditions. An adiabatic total-to-total efficiency of 92.1% with expansion ratio of 4.47 at design point is obtained and achieves the initial design goal very well. The paper is aimed at providing a technical approach to improve the thrust weight ratio, efficiency of high bypass turbofan engines, and provide new ideas for the development of aeroengines.

1. Introduction

As the core of aerospace aircraft, the engine directly reflects the overall development level of aerospace technology [1]. Thrust-to-weight ratio and efficiency are two important performance parameters to evaluate the development level of an aircraft engine. As an important component of the engine, the turbine has direct impact on the engine. The counter rotating turbine as an advanced technology can significantly improve the thrust-to-weight ratio, efficiency compactness, reliability, and maintainability of the engine. Moreover, the manoeuvrability is also improved [2–5].

Counter rotating turbine is a turbine in which two adjacent rotors rotate in opposite directions [6, 7]. Wintucky and Stewart [8] were the first to investigate counter rotating turbine technology, mainly through theoretical analysis of the relationship between efficiency and the turbine speed ratio and output power ratio. They also showed that the efficiency of a 1 + 1/2 counter-rotating turbine is 2 ~ 4% higher than that of a conventional two-stage turbine when the low-pressure turbine inlet guide vane is eliminated. In addition, the HPT and LPT speed ratio has little effect on the maximum efficiency of the turbine, but it affects the output work distribution of the HPT and LPT at the maximum efficiency of the turbine. A similar study was performed by Louis [2], which presented a theoretical analysis of 1 + 1/2 and 1/2 + 1/2 counter rotating turbine. The researchers concluded that the flow angle of the counter rotating turbine is smaller, and the efficiency is higher when the stage loading coefficient is same. In other words, the stage loading coefficient of counter rotating turbine is greater than that of the conventional turbine at the same efficiency. Similarly, Sotsenko and Ponomariov [9–11] concluded that the technology of counter rotating turbine without guide vanes can increase the turbine inlet temperature by approximately 60 K, directly increasing the engine thrust-to-weight ratio.

In the counter-rotating turbine's experimental study, Yamamoto and Outa [12, 13] proposed a low-speed and high-loading counter-rotating turbine to improve output power. The speed of HPT and LPT is 1500 rpm. The number of two counter rotating rotors and inlet guide vanes is 16. The rotor cascade adopts the extremely high-loading design with turning angle of 160°. The cascade test results showed that the actual turning angle is 146° with a significant deviation angle. In addition, the schlieren diagram shows that there is no significant difference in the flow structure between the large turning angle cascade and the conventional small turning angle cascade, but there are strong channel vortices in the large turning angle cascade, with greater downstream mixing losses and flow losses.

For the counter rotating turbine used in rocket turbopump, Huber et al. [14] studied the small-size, high-speed counter rotating turbine. The counter rotating turbine casing has an outer diameter of 4.1 inches and a blade height of 0.25 inches. The counter rotating turbine is characterized by small size, small mass flow, and high output power. Due to the requirements of small mass flow and large output power, the HPT blades have a geometric turning angle of up to 160°. Tests were carried out to compare and analyze the LPT with and without inlet guide vanes. The study shows that without inlet guide vane, the turbine efficiency can be increased by 2%, and the total turbine efficiency can reach 0.80.

According to many studies of counter-rotating turbines, the Mach number at the outlet of the HPT blade is supersonic along spanwise. The variable geometry of the inlet guide vane is the most efficient method of adjusting the engine's operating conditions. Haldeman et al. [15] conducted an experimental and numerical simulation study of a 1 + 1/2 counter-rotating turbine and demonstrated that the experimental and numerical results agreed well, with only minor deviations at the rotor's trailing edge. Due to the influence of the upstream HPT outlet wake, the blade surface of the LPT in the counter-rotating turbine is subject to a wide range of unsteady stress. Keith et al. [16] conducted an experimental research on an advanced counter-rotating turbine (controllable pressure ratio turbine (COPE)) in the same year. The advanced counter-rotating turbine is characterized by the adjustable inlet guide vanes of the HPT, the high-loading transonic rotor, and the counter-rotating aerodynamic layout. The test results indicate that the adjustable guide vane has little impact on the aerodynamic performance. Under the variable geometry of the guide vane, HPT has reached its maximum efficiency, and the performance of the test turbine matches the forecast. Wu et al. [17, 18] pointed out the operating characteristics of 1 + 1/2 and 1 + 3/2 counter-rotating turbines under design and off-design conditions and highlighted the various operating characteristics of HPT and LPT.

In the study of aerodynamic characteristics of the counter rotating turbine, the high Mach number (1.4 ~ 1.7) at the outlet of the rotor creates a complex flow dominated by shock wave, compression wave, and expansion wave. In addition, the counter rotating of rotors results in a significant increase in the relative speed, which is approximately twice that of the traditional turbine, and the flow field characteristics of the counter-rotating turbine will invariably exhibit strong unsteady characteristics. Wang et al. and Zhao et al. [19–21] analyzed the wave system of the 1 + 1/2 counter rotating turbine. Suction side pressure waves (sspw) are generated near approximately 60% of the axial chord length of the HPT rotor, and their intensity is diminished after passing the inner edge shock (IES) of the adjacent blade trailing edge. The IES-reflected shock wave is still powerful and cannot be disregarded, and the outer edge shock (OES) extends the downstream. It can be seen from the wave distribution that the LPT will face complex conditions. By means of high-resolution large eddy simulation, Zhao and Sandberg [22] also demonstrated that the major loss in a counter-rotating turbine is due to the interaction between the boundary layer and shock wave [23].

The development process of the dual-shaft aeroengine turbine is examined in order to explore the turbine novel aerodynamic layout. The HPT and LPT rotate in the same direction (corotating) during first phase. Second, the HPT and LPT rotate in opposite directions (counter-rotation), while the LPT inlet guide vane remains unchanged. As corotation develops to counter-rotation, the turning angle and solidity of the LPT inlet guide vane are drastically reduced, which is advantageous for the turbine efficiency and weight. Third, the LPT inlet guide vanes are eliminated entirely, removing the loss and weight associated with the guide vanes and further enhancing the thrust-to-weight ratio and efficiency.

To meet the future demand for a higher thrust-to-weight ratio and efficiency, a breakthrough in the turbine layout will be necessary. In conventional counter-rotating turbines, the HPT is located in the front of the LPT, and only one stator row can be removed. The layout prevents the turbine from becoming lighter and more efficient. Therefore, the staggered counter rotating turbine is proposed, and the layout of the staggered counter rotating turbine is depicted in Figure 1 The staggered counter-rotating turbine can eliminate all-internal stators, drastically reduce the turbine weight, and increase its efficiency. The organization of the paper's content is as follows: Section 2 describes the aerodynamic design of the staggered counter-rotating turbine, outlining the meanline analysis and flowpath analysis. Subsequently, Section 3 presents the principal outcomes of the performance evaluation of the staggered counter-rotating turbine, along with numerous discussions. Section 4 presents the investigation's concluding remarks and perspectives for the future.

2. The Staggered Counter Rotating Turbine Aerodynamic Design

2.1. Meanline Analysis. Whether it is a conventional or counter-rotating turbine design, the selection of the velocity triangle is crucial to the preliminary design, and a reasonable velocity triangle is a prerequisite for a successful turbine design. Counter-rotation reduces the downstream rotor's degree of freedom by one compared to a conventional turbine, thereby limiting the optimal choice of aerodynamic design parameters. The constraint causes the counter-rotating

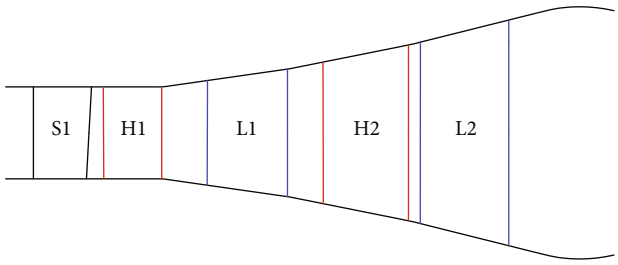

Figure 1: Staggered counter rotating turbine.

turbine's aerodynamic design to exhibit new characteristics. Conventionally, the velocity triangle of the first stage blade is determined by five independent variables. Internal stators are eliminated from the staggered counter-rotating turbine, and the outlet of the upstream rotor is the inlet of the downstream rotor. Therefore, there are now three independent variable parameters for the subsequent stage. The selection of the independent variables is various. In this paper, however, the commonly independent variables in turbine design are chosen: the loading coefficient, the reaction, the absolute flow angle, the axial velocity ratio, and the output work. Then, in the internal stage, the loading coefficient, axial velocity ratio, and output work are selected. The flow angles proposed in this paper are axial angles with an absolute value.

2.1.1. Increasing Rotor Outlet Swirl. For the staggered counter rotating turbine, the main concern is how to provide sufficient swirl for the downstream rotor due to the eliminated stator. It can be known from the reaction and loading coefficient equation that

$$Ht = \frac{Lu}{U^2}, \tag{1}$$

$$\Omega = 1 - \frac{C_2^2 - C_1^2}{2Lu}. \tag{2}$$

According to the Euler equation $Lu = U(C_{1u} + C_{2u})$ and the triangle equation $C^2 = C_a^2 + C_u^2$, the following formula can be obtained:

$$C_{2u} = \frac{\sqrt{LuHt}}{2} + \sqrt{\frac{Lu}{Ht}}(\Omega - 1). \tag{3}$$

As can be seen in Equation (3), the outlet swirl C_{2u} is proportional to the Lu and Ω. Therefore, increasing the rotor outlet swirl requires the blade output work and reaction to increase. This explains why the conventional counter-rotating turbine high-pressure stage is designed with a reaction degree greater than 1. In addition, the Equation (3) shows that the loading coefficient which minimizes the outlet swirl is existed. According to the mathematical analysis, when Ht is equal to $\Omega - 1$, the rotor outlet swirl reaches the minimum, and the loading coefficient is less than 1 when the minimum is reached. In conventional turbine design, the loading coefficient is usually greater than 1 to make full use of circumferential velocity. According to the trend of the swirl curve, it can be concluded that the rotor outlet swirl is also proportional to the loading coefficient Ht.

The above analysis can be applied to the design parameters selected for the first stage of the staggered counter-rotating turbine. However, the internal stages are vaneless, and the inlet of the downstream rotor is the outlet of the upstream rotor. According to the Euler equation, the outlet swirl is directly proportional to the internal stages' turbine output work.

2.1.2. Decreasing Rotor Outlet Mach Number. The selection of design parameters needs to coordinate the Mach number of the turbine rotor outlet. If the Mach number is too large, it can be reduced through the following method. According to the turbine velocity triangle

$$W_2^2 = C_{2a}^2 + (C_{2u} + U)^2. \tag{4}$$

Combined with the axial velocity ratio K and the absolute flow angle α at the inlet, the following formula can be obtained:

$$W_2^2 = \left(\frac{K \cdot C_{1u}}{\tan \alpha}\right)^2 + (U + C_{2u})^2. \tag{5}$$

When the loading coefficient, reaction, and output work are selected, namely, C_{1u}, C_{2u}, and U, the outlet relative velocity can be decreased by increasing the inlet absolute flow angle or decreasing the axial velocity ratio. However, the expansion angle of the flowpath must also be considered when selecting the axial velocity ratio. If the expansion angle is too great, it can cause the endwall boundary layer to separate. The expansion flowpath design between vaneless rotors is an additional effective method for reducing the rotor outlet Mach number. The expansion flowpath can reduce the axial velocity and increase the inlet flow angle of the downstream rotor, which is advantageous for decreasing the relative Mach number at the outlet of the rotor.

2.1.3. Decreasing Turbine Outlet Flow Angle. The section arrangement and the designations of the staggered counter-rotating turbine are shown in Figure 2. Different subscript numbers represent different calculation sections.

The turbine outlet flow angle has an important influence on the aerodynamic performance of the downstream nozzle. According to the change in the tangential velocity, the following formula can be obtained:

$$C_{2u} = \Delta C_{uH1} - C_{1u}, \tag{6}$$

$$C_{4u} = \Delta C_{uL1} - C_{3u}, \tag{7}$$

$$C_{6u} = \Delta C_{uH2} - C_{5u} \tag{8}$$

$$C_{8u} = \Delta C_{uL2} - C_{7u}, \tag{9}$$

According to the above formulas and the condition that the inlet of the downstream rotor is the outlet of the upstream rotor, the outlet swirl is

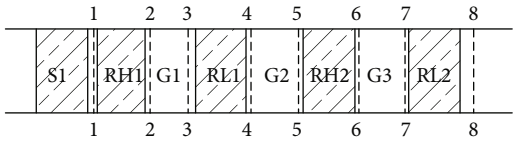

Figure 2: Schematic diagram of a staggered counter-rotating turbine.

$$C_{8u} = \Delta C_{uL1} + \Delta C_{uL2} - (\Delta C_{uH1} + \Delta C_{uH2}) + C_{1u}. \quad (10)$$

Combined with the Euler equation, the above formula becomes

$$C_{8u} = \frac{L_{uL1}}{U_{L1}} + \frac{L_{uL2}}{U_{L2}} - \left(\frac{L_{uH1}}{U_{H1}} + \frac{L_{uH2}}{U_{H2}}\right) + C_{1u}. \quad (11)$$

Since the design of the turbine adopts the iso-middle diameter design, and then $U_{L1} = U_{L2} = U_L$, $U_{H1} = U_{H2} = U_H$, and then

$$C_{8u} = \frac{Lu_L}{U_L} - \frac{Lu_H}{U_H} + C_{1u}. \quad (12)$$

$Lu_L = Lu_{L1} + Lu_{L2}$ is the output work of LPT, and $Lu_H = Lu_{H1} + Lu_{H2}$ is the output work of HPT. The rotational speed ratio is $K_{LH} = U_L/U_H$.

$$C_{8u} = \frac{Lu_L/K_{LH} - Lu_H}{U_H} + C_{1u}. \quad (13)$$

It can be seen from the equation that when the rotational speed ratio is equal to the power output ratio, namely, $U_L/U_H = Lu_L/Lu_H$, no matter how the work is distributed between HPT and LPT, the turbine outlet swirl is equal to the HPT rotor inlet swirl. Therefore, in order to make the turbine outlet flow angle equalled to zero, the inlet of the HPT first rotor should be the axial. However, according to the analysis above, when the inlet of HPT rotor is axial, the Mach number at the outlet of high-pressure turbine blade is large. Therefore, in order to reduce the Mach number at the outlet of the HPT rotor, the proper swirl must be implemented while keeping the turbine outlet flow angle within an acceptable range.

In addition, when $U_L/U_H = Lu_L/Lu_H$, according to the Euler equation,

$$\Delta Cu_H = \Delta Cu_L. \quad (14)$$

When the blade output work distribution is equal, respectively, for HPT and LPT, namely $Lu_{H1} = Lu_{H2}$, $Lu_{L1} = Lu_{L2}$, from Equation (14), the following formula can be obtained:

$$\Delta Cu_{H1} = \Delta Cu_{L1} = \Delta Cu_{H2} = \Delta Cu_{L2}. \quad (15)$$

From Equations (6)–(8), the following formula can be obtained:

Table 1: Staggered counter-rotating model turbine performance requirements.

	HPT	LPT
Inlet total pressure/MPa	0.5	
Inlet total temperature/K	400	
Speed/RPM	20124	13111
Mass flow/kg/s	3.72	3.72
Work/kW	>280	>180
Total-total adiabatic efficiency	0.9	0.9
Outlet flow angle/deg	<25	

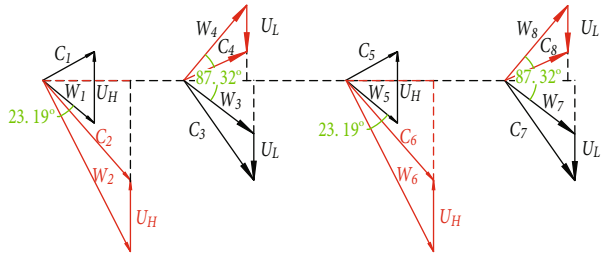

Figure 3: Velocity triangles at meanline section.

Table 2: Turbine meanline design parameters.

	H1	L1	H2	L2
Stage pressure ratio (π)	1.55	1.34	1.63	1.43
Stage flow coefficient (Φ)	1.2	0.88	1.2	0.88
Stage work coefficient (Ψ)	1.8	1.2	1.8	1.2
Relative inlet flow angle (α)	-39.7	37.3	-39.7	37.3
Relative exit flow angle (β)	-62.9	-50	-62.9	-50
Rotor axial velocity ratio (K)	1.7	0.9	1.7	0.9
Duct axial velocity ratio	0.8	0.82	0.8	

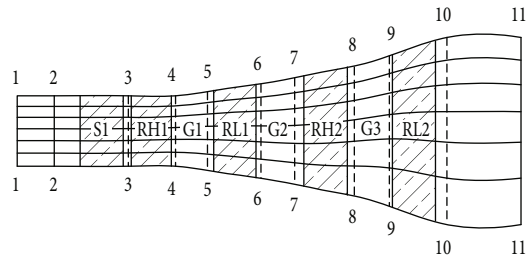

Figure 4: Meridian streamline.

$$\begin{aligned} C_{1u} &= C_{5u}, \\ C_{2u} &= C_{6u}, \\ C_{3u} &= C_{7u}, \\ C_{4u} &= C_{8u}. \end{aligned} \quad (16)$$

The Equation (16) shows that the HPT rotors are designed with the same velocity triangle under the same axial velocity, that is, the repetitive stage design. Similarly, the LPT is also a repetitive stage design. The repetitive stage

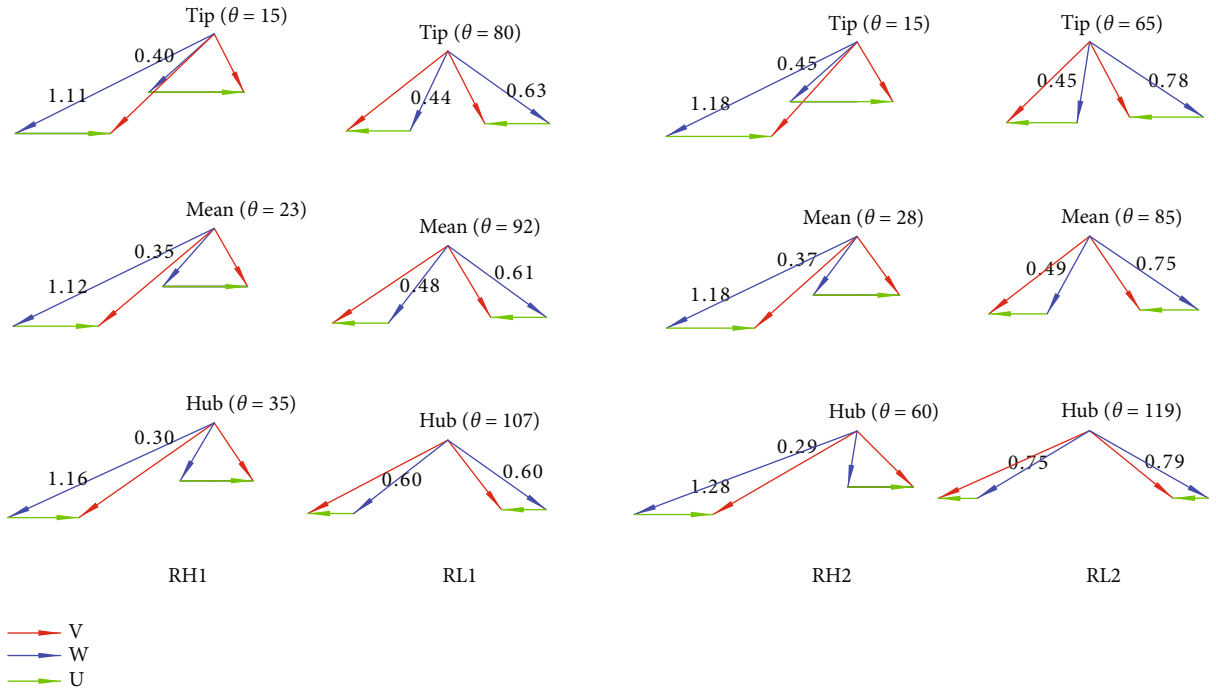

Figure 5: Velocity triangle.

design can significantly reduce the processing cost and maintenance cost.

If $Lu_L/Lu_H > U_L/U_H$, it can be seen from the Equation (13) that the outlet flow angle of the turbine is always positive. And the turbine outlet flow angle is not related to the LPT work distribution. It is important to note, however, that the turbine outlet flow angle is related to the HPT work distribution. This is because, when the first rotor loading coefficient of the HPT is given, the greater the output work, the greater the circumferential velocity of the HPT, and the smaller the turbine outlet flow angle. From the above analysis, it can be seen that the staggered counter rotating turbine cannot obtain zero flow angle under the condition of $Lu_L/Lu_H > U_L/U_H$, unless the first rotor of HPT adopts negative swirl design, but this is unrealistic. Therefore, to obtain the minimum turbine outlet swirl, it requires reducing the first rotor inlet swirl of the HPT as well as increasing turbine rotation speed.

If $Lu_L/Lu_H < U_L/U_H$, it can be seen from the Equation (13) that the inlet flow angle and HPT work distribution can make the outlet flow of LP turbine axial, but the relationship does not make full use of turbine speed.

Based on the above analysis and the conventional HPT and LPT performance requirements, this paper proposes that the staggered counter-rotating model turbine performance requirements are shown in Table 1. The aerodynamic performance requirements proposed are based on the similarity theory and the specifications of the model turbine test platform in our laboratory, so as to carry out the model turbine test research on the staggered counter rotating turbine in the future.

The meanline design space is explored by parametrically varying rotor loading coefficient, axial velocity ratios of blades and ducts, etc., to achieve a satisfactory meanline velocity triangle diagram under the condition of $Lu_L/Lu_H = U_L/U_H$, and the repetitive stages design is adopted. The resulting relative Mach number triangles at the leading edge and the trailing edge of rotors as well as flow deflection angles are given in Figure 3. Since the ducts decelerate the gas flow before rotors, the absolute Mach number of the inlet flow of a rotor is smaller than that of its upstream rotor, rather than identical with that. The relative exit Mach numbers of all the rotors are greater than unity, indicating that the control of shock losses and shock-induced boundary layer separation might be a key technique for the staggered counter rotating turbine design. The small turnings of the flow in R1 and R4 contribute significantly to the efficiency of the stage by reducing secondary flow losses. The mean line design results of the turbine are shown in Table 2.

Table 3: Meridional design parameters.

	H1	L1	H2	L2
Aspect ratios (based on axial chord)	1.60	2.1	2.9	3.8
Hub tip ratio	0.77	0.71	0.62	0.51

2.2. Throughflow Analysis. Streamline curvature throughflow calculation is then performed to determine the blade conditions for 3D blading. Notably, two calculation stations are positioned between two adjacent rotors so that the calculation program can solve the expansion duct, thus decreasing the Mach number of the downstream rotor. In the calculation program, all rotors adopt the equal work distribution along the radial direction, and the inlet total temperature

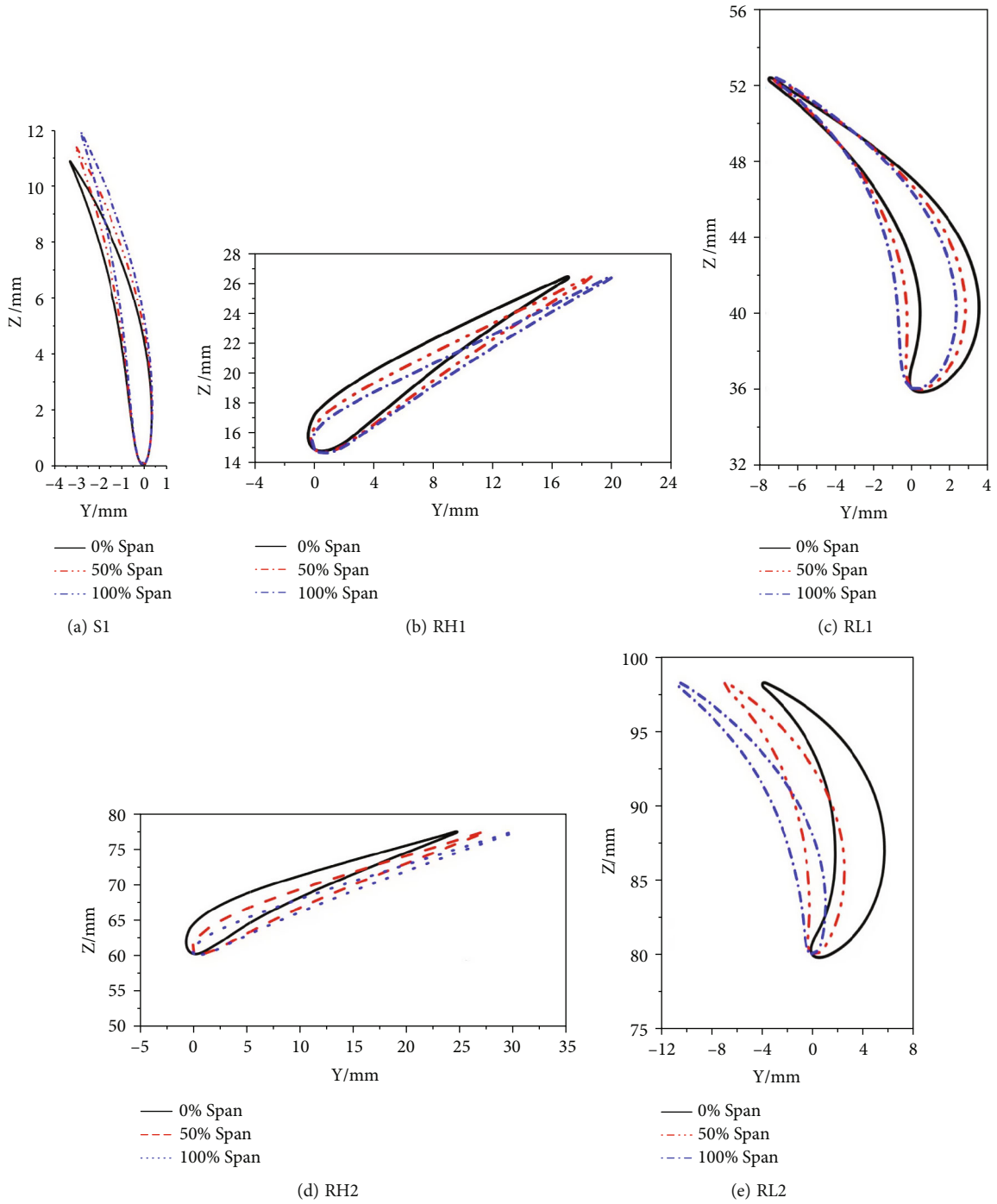

Figure 6: Blade profiles at tip, midspan, and root for S1, RH1, RL1, RH2, and RL2.

and pressure are uniformly distributed along the radial direction, the turbine blade loss model adopts the KO model, and the tangential velocity of the turbine guide vane outlet is given according to the equal circulation distribution. The meridian streamline calculated by the program is shown in Figure 4, and the velocity triangle distribution is shown in Figure 5. All the relative Mach numbers increase across the blade sections.

The chord lengths of blade mean sections should be as short as possible. Internal axial gaps are determined based on the duct flare angles with a maximum value of 15 deg to avoid endwall boundary layer separation. The final meridional design results are presented in Table 3, and the schematic sketch of the meridional flowpath is shown in Figure 5.

2.3. 3D Blade. Blade channel shapes should be designed to achieve velocity distributions without boundary layer separation during the profile design process. Each blade geometry is divided into five two-dimensional sections with a

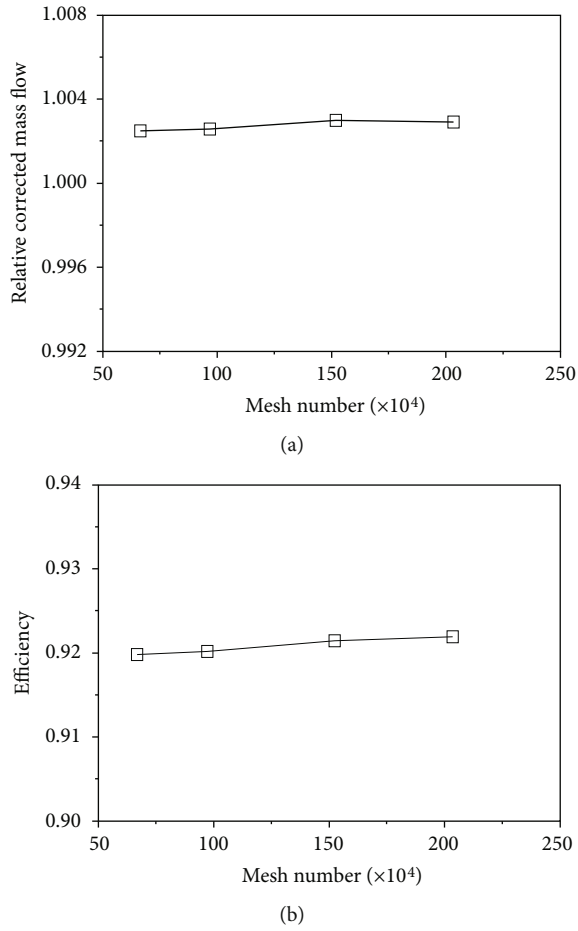

Figure 7: Grid-independence verification.

radial interval of approximately 25 percent of blade height. Then, the three-dimensional geometry of the rotor blade is created by stacking these two-dimensional blade section profiles radially through their respective centers of gravity. Since the flow in the rotor of the turbine is transonic with a relative exit Mach number between 1.0 and 1.3, convergent blade passages are constructed for each blade section with a throat that begins at the trailing edge and ends on the suction side. The throat areas are determined by the continuity equation. Iteratively optimizing the blade pressure and suction curves prevents flow separation. The tip, the midspan, and the root blade profiles are shown in Figure 6.

3. Analysis of Aerodynamic Performance and Operating Characteristic

3.1. Numerical Algorithm. In this paper, the NUMECA software package, a general computational fluid dynamics software for turbomachinery, is used to solve the three-dimensional steady Reynolds averaged Navier-Stokes equations and obtain the detailed characteristics of the turbine. To discretize the control equations, the finite volume method is used, the central difference scheme with second-order accuracy is used for spatial difference, and the fourth-order Runge-Kutta method is used for time advance. As the turbulence model, the Spalart-Allmaras (S-A) one-equation model is selected. In turbomachinery, the S-A turbulence model can accurately predict the separated flow and shock wave. At the interface between blades, the mixed plane (MP) method is utilized to process the data. In the numerical simulation, it is presumed that the boundary layer has fully developed. It is assumed that the wall is adiabatic. Implicit residual smoothing and multigrid techniques are used to accelerate convergence. The inlet boundary condition is determined by the distribution of total temperature, total pressure, and velocity vector. Average static pressure defines the outlet boundary condition. When calculating the off-design-point flow state, the inlet boundary condition parameters are maintained while the outlet static pressure is altered.

Numeca/autogrid is used to automatically generate the structured grid. As shown in Figure 7, the grid-independence verification reveals that the mass flow rate difference is 0.1 percent, and the efficiency difference is 0.25 percent for grid numbers 60104 versus 200104. In order to analyze the performance of a staggered counter-rotating turbine, as depicted in Figure 8, the grid number 60104 has been chosen for this paper. The maximum dimensionless wall length Y+ is 15 (Figure 9), which is predominantly distributed at the top gap of the HPT blade. This y + distribution satisfies the requirements of the S-A turbulence model for

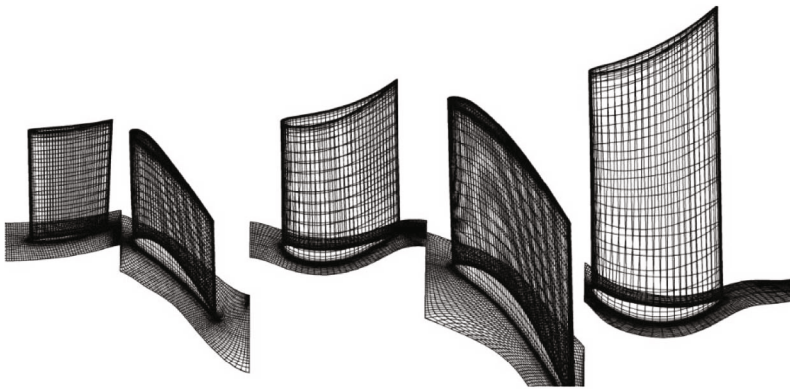

(a) Staggered counter-rotating turbine 3D grid

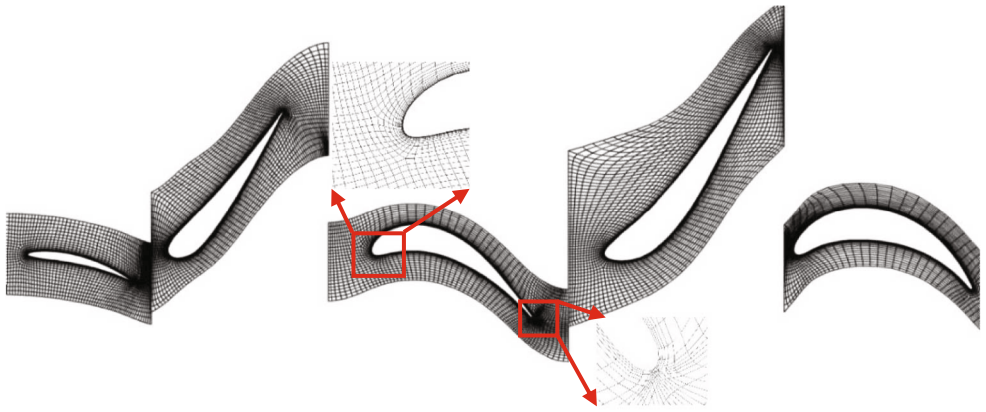

(b) Blade root grid

Figure 8: Staggered counter rotating turbine blade gridM.

the first layer of grid thickness on the wall [24]. And all performance parameters are calculated by mass flow weighted average.

3.2. Flow Field Characteristics. The spanwise distribution of relative flow angle and relative Mach number at the center of each blade outlet duct is depicted in Figure 10. The relative Mach number at the RH1 and RH2 blades remains greater than 1.0 even when the expanding flowpath is adopted, and all the Mach number along the spanwise is greater than 1.0. This indicates that the downstream disturbance cannot be transmitted through the RH2 blade to the upstream, and that the operation state of the upstream turbine cannot be altered by the backpressure, which is a significant departure from the conventional turbine. The Mach number distribution also reveals that the key technologies in the staggered counter-rotating turbine design are the control of shock wave and shock-induced boundary layer separation loss. The spanwise relative flow angle distribution reveals that the root and tip of RL1 and RL2 blades are over swirling, primarily due to the passage vortex, whereas the tip of RH1 and RH2 blades is under swirling, primarily due to the leakage flow.

The relative Mach number contour at 50% blade height for the staggered counter rotating turbine is depicted in Figure 11. Even though the outlet flow of the HPT blades is supersonic, there is no obvious boundary layer separation caused by shock waves. The primary reason is that the blade profile design behind the throat features a straight line, which reattaches the separated boundary layer and prevents it from thickening and separating further. For the two high-pressure turbine rotors, the flow sonic line can be seen inside the blade flow passage, which begins at the leading edge of the rotor suction surface and ends close to the trailing edge, and has a highly curved state. This highly curved state indicates that the flow of the HPT rotors has completed the majority of flow turning and expansion at the leading edge, with only a small portion of expansion and acceleration occurring after the throat. The leading edge of the rotor exhibits a substantial aerodynamic loading distribution. However, inside the flow passage of LPT rotors, there is no sonic line that is conducive to operating adjustment. The relative Mach number at the LPT rotors' inlet and outlet is low. However, there is an obvious region of high Mach number near the leading edge of the suction surface, and the flow behind this region appears to be in a deceleration flow state, which is directly conducive to the thickening and separation of the boundary layer on the suction surface, and flow loss will increase. The reason may be that the number of the first rotor of the LPT is decreased in order to meet the power output requirements of the first stage blade of the HPT, thereby increasing the loading.

The flow state on the blade surface may be simply understood from the loading distribution, and Figure 12 depicts

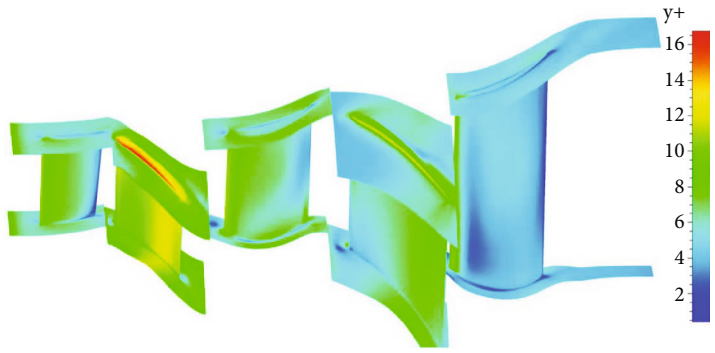

Figure 9: Wall Y + distribution.

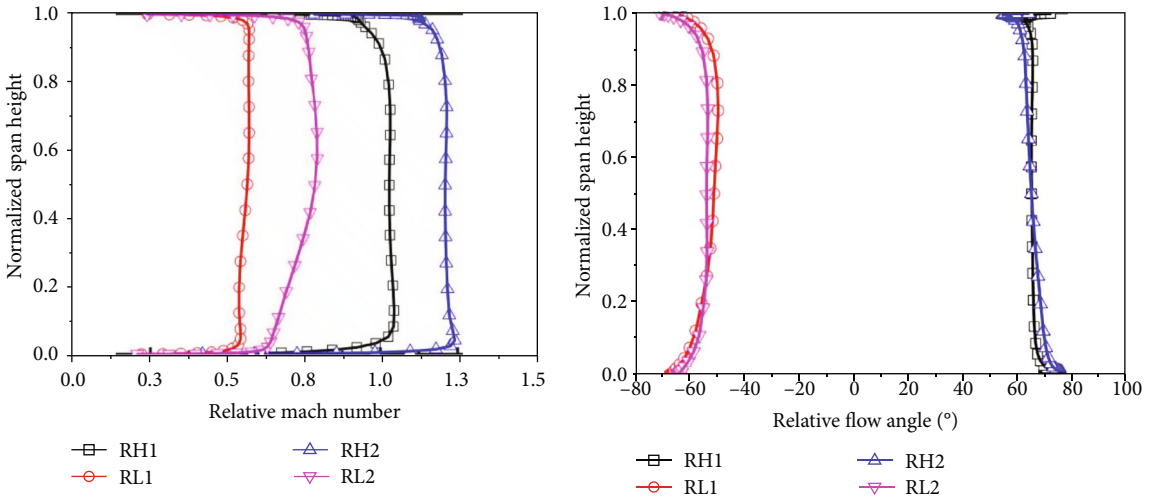

(a) Relative Mach number

(b) Relative flow angle

Figure 10: Relative Mach number and flow angle distribution along the span.

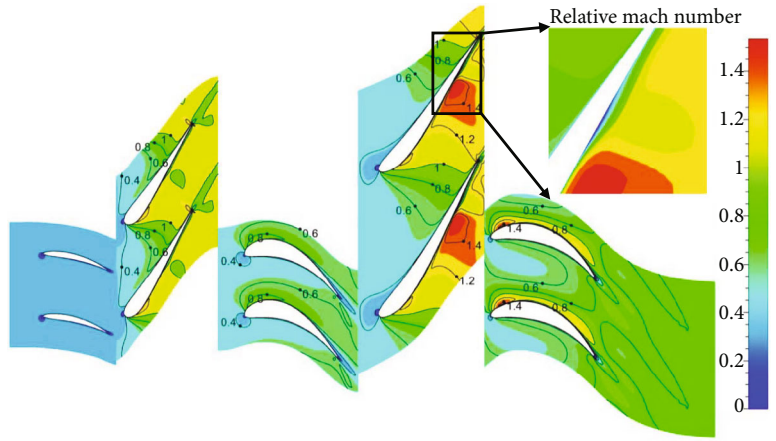

Figure 11: Relative Mach number contour at 50% blade height.

the static pressure distribution at the spanwise middle section. Additionally, the S1 static pressure distribution reveals a reverse pressure gradient close to the trailing edge. The static pressure distribution on the suction surface of RH1 and RH2 differs substantially from that of a normal turbine rotor. The fluctuating static pressure on the suction surface suggests that the boundary layer flow is accelerating and decelerating. The primary cause is the supersonic Mach number at the rotor's outlet, which causes the interplay of expansion wave, shock wave, reflected expansion wave, and reflected shock wave in the flow channel. Therefore, it is required to organize the shock wave dispersion in the rotor

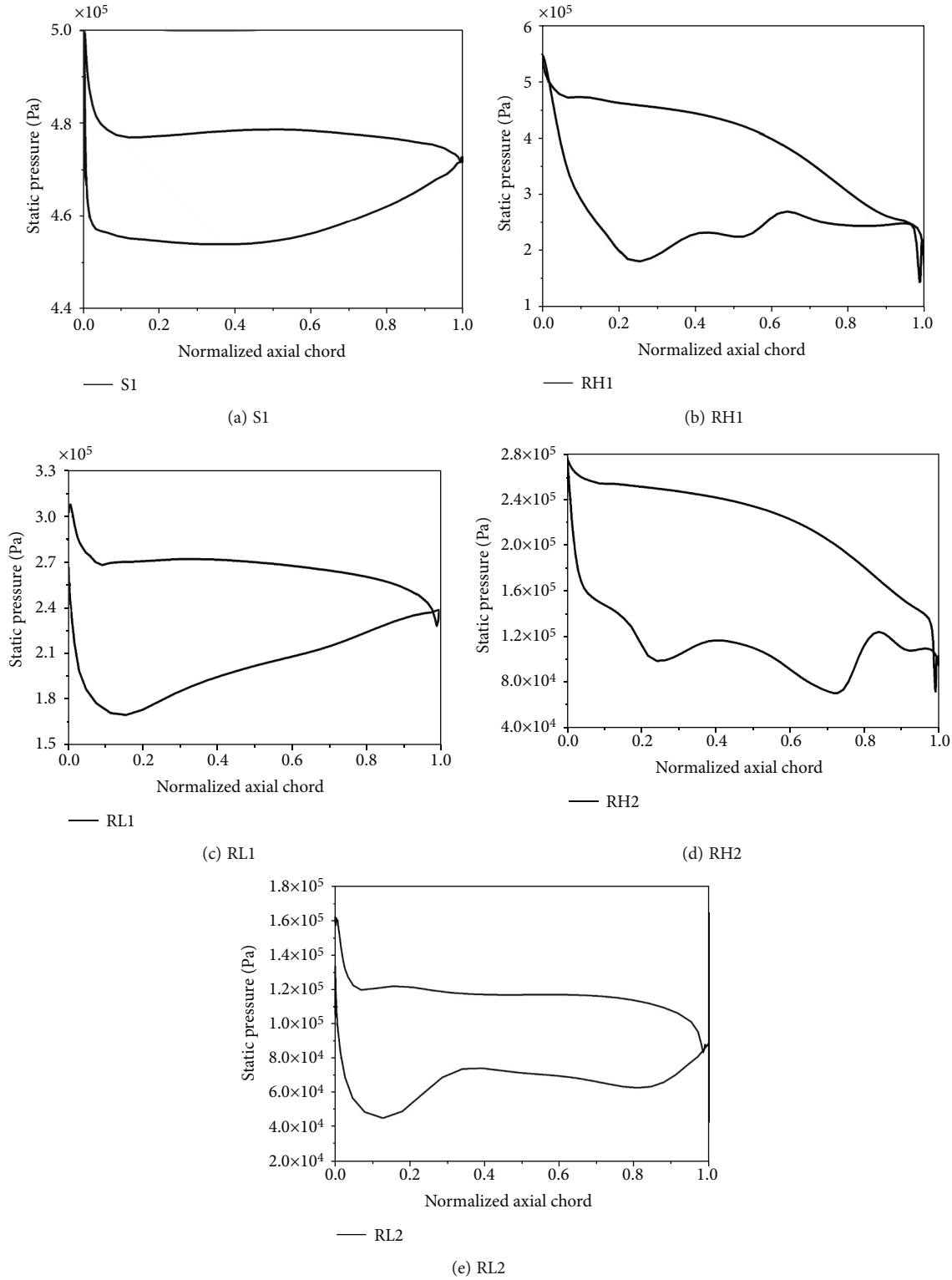

Figure 12: Static pressure distribution.

channel in a reasonable manner. In addition, it is important to note that the static pressure on the suction surface of RL1 rises steadily behind the leading edge, indicating that the boundary layer on the suction surface tends to thicken and separate. In Figure 11, the Mach number contour also reveals that boundary layer separation has occurred at the leading edge. The static pressure on the suction surface of RL2 progressively increases from approximately 10% of the axial chord length to 40% of the axial chord length. It demonstrates that a set of compression waves exists at approximately 10% of the axial chord length, which gradually thickens the low-energy fluid in the blade boundary layer.

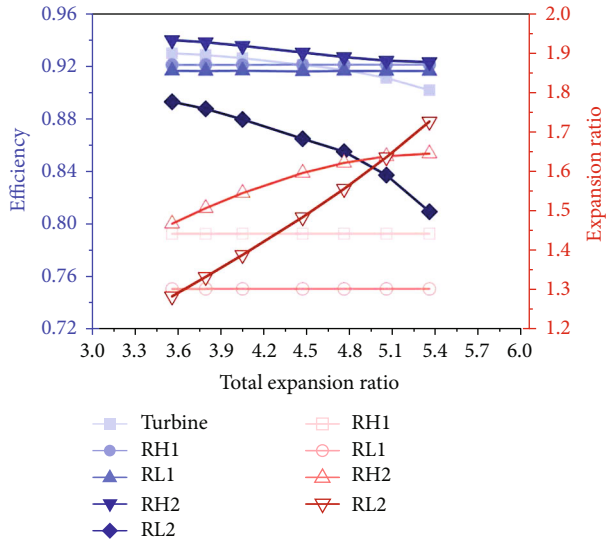

Figure 13: Efficiency and expansion ratio distribution.

In the staggered counter-rotating turbine, shock wave loss and shock wave-induced boundary layer separation loss are evidently the primary losses.

3.3. Turbine Operating Performance. At the design point, the total expansion ratio of the turbine is 4.47, the total-total adiabatic efficiency of the turbine according to the Equation (17) is 0.921, of which the HPT first rotor (H1) is 0.921, the LPT first rotor (L1) is 0.917, the HPT second rotor (H2) is 0.936, the LPT second rotor (L2) is 0.865, and the flow mass is 3.729 kg/s.

$$\eta^* = \frac{T_1^*/T_K^* - 1}{1 - 1/\pi_K^{*\,k-1/k}}. \tag{17}$$

To analyze the efficiency and expansion ratio distribution of each turbine stage at the design speed, Figure 13 depicts the efficiency and expansion ratio distribution diagram. It is evident from Figure 13 that the RL2 has a relatively low level of efficiency. As the growth ratio increases, the efficiency declines quite rapidly. When the expansion ratio of the turbine hits 5,4, the RL2's efficiency drops to approximately 0.80. In addition, it is important to note that the expansion ratio, efficiency, and turbine mass flow (Figures 13–14) of the RH1, RH2, and RL1 rarely alter with the turbine's overall expansion ratio. The primary reason is that the RH2's throat is in a sonic condition along the spanwise direction; therefore, disturbances downstream cannot be conveyed upstream. RH2 has an expansion ratio that is nearly linear with the total expansion ratio. Therefore, it is crucial to develop RH2 with high efficiency across a broad expansion ratio range.

To investigate the operation characteristics of the turbine at different speeds, the mass flow characteristics of the turbine are depicted in Figure 15. The mass flow characteristics reveal that the mass flow of the turbine varies little with the expansion ratio, which is consistent with the study presented previously. In addition, differing LPT speeds have minimal

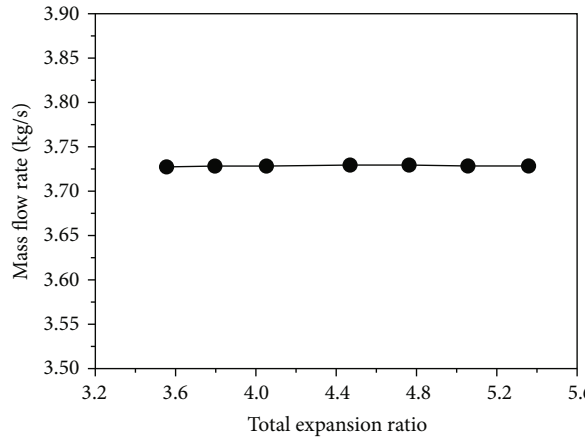

Figure 14: Mass flow characteristics at design speed.

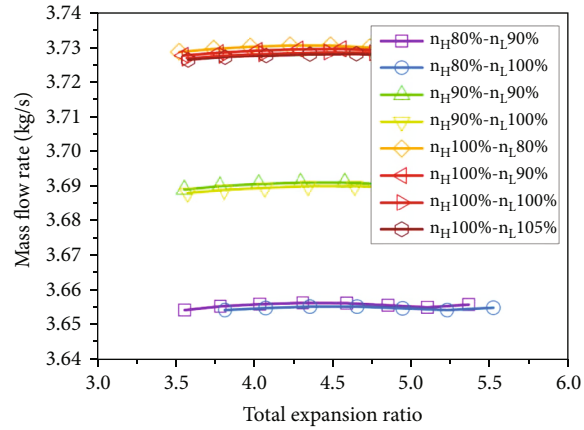

Figure 15: Mass flow rate characteristics at different speeds.

impact on the mass flow, although HPT speeds do. The primary reason is the fact that RH1 largely determines the turbine mass flow rate. At different LPT speeds, the throat of the RH1 is sonic state. The LPT speed variation corresponds to a RH1 disturbance. This disturbance is unable to travel through the HPT throat and alter the mass flow. In addition, the speed of the HPT increases the flow of the turbine, which differs from the normal turbine. In a typical turbine, the turbine speed decreases the mass flow rate. The primary reason for this distinction is because the throat of the turbine is located at RH1, whereas the throat of traditional transonic turbines is located at the guiding vane.

4. Conclusions

This paper presents the design philosophy and the performance analysis of the staggered counter-rotating turbine. The major conclusions of the present study may be summarized as follows:

(1) Since there are no of vanes in front of the rotor blades, the aerodynamic design of the staggered turbine suffers from insufficient inlet swirls. Both increasing the stage loading and reaction of the upstream rotor and decreasing the axial velocity

ratio of the upstream duct are efficient methods for enhancing the inlet swirls of the succeeding rotor blades. However, the former does this at the expense of increasing the relative exit Mach number of the upstream rotor, whilst the latter demands a higher axial gap in the duct in order to lower the expansion angles and avoid endwall boundary layer separation

(2) The turbine output angle is also an essential criterion for evaluating the turbine design. The below methods can be adopted to reduce the flow angle. When the HPT and LPT speed ratio is equal to the output work ratio, the RH1 adopts the axial inlet design, which can guarantee the flow angle equal to zero. When the HPT and LPT speed ratio is greater than the output work ratio, reducing the inlet swirl of RH1 and increasing the HPT speed can reduce the flow angle. However, at this situation, the flow angle cannot equal to zero. In addition, when the HPT and LPT speed ratio is equal to the output work ratio, the HPT and LPT can adopt the same blade design, which can reduce the cost

(3) The Mach number at HPT rotor outlet is supersonic, and there are complex shock wave structures in the flow passage. It is necessary to reasonably arrange the shock wave distribution in the flow passage. Controlling shock wave distribution is the key technology at the staggered counter rotating turbine design

(4) The design turbine meets the performance specifications. The efficiency of the RL2 is relatively low. As the expansion ratio increases, the efficiency declines quite rapidly. In addition, the expansion ratio, efficiency, and turbine mass flow of the RH1, RH2, and RL1 rarely vary with the total expansion ratio. The main influence of the total expansion is the expansion ratio of the RL2. Therefore, it is very important to design RL2 with high efficiency in a wide range of expansion ratio. Different LPT speeds have little effect on turbine mass flow characteristic, but HPT speed has. With the increase of HPT speed, the mass flow rate increases. The operating conditions of the downstream turbine have no effect on the operating characteristics of the upstream turbine

Nomenclature

Symbols

C: Absolute velocity
U: Circumferential velocity
Lu: Output work
W: Relative velocity
α: Absolute flow angle
β: Relative flow angle
Ht: Loading coefficient
Ω: Reaction
K: Axial velocity ratio
η: Adiabatic isentropic efficiency
γ: Passage expansion angle
G: Duct
H: High-pressure turbine
L: Low-pressure turbine
π: Pressure expansion ratio
k: Specific heat ratio

Subscripts

a: Axial component
u: Tangential component
1: First rotor inlet
2: First rotor outlet
3: Second rotor inlet
4: Second rotor outlet
5: Third rotor inlet
6: Third rotor outlet
7: Fourth rotor inlet
8: Fourth rotor outlet

Abbreviations

HPT: High-pressure turbine
LPT: Low-pressure turbine.

Data Availability

The data presented in this study is available on request from the corresponding author.

Conflicts of Interest

The authors declare that there is no conflict of interest regarding the publication of this paper.

Acknowledgments

This work has been supported by the Hainan Natural Science Foundation High Level Talent Program (Grant No. 520RC533) and the Hainan Innovation Team Program (Grant No. 422CXTD509).

References

[1] K. Wang, Y. Q. Guo, and W. L. Zhao, "Analysis of scrapping characteristics and reliability of civil aero engine high pressure turbine blade in dual failure modes," *Journal of Beijing University of Aeronautics and Astronautics*, vol. 37, pp. 1–13, 2022.

[2] J. F. Louis, "Axial flow contra-rotating turbines," in *Proceedings of the ASME 1985 International Gas Turbine Conference and Exhibit. Volume 1: Aircraft Engine; Marine; Turbomachinery; Microturbines and Small Turbomachinery*, Houston, Texas, USA, 1985.

[3] K. Zhou, Z. Zou, H. Liu, and L. Wang, "Aerodynamic design of counter-rotating turbine for aero-engine," *Science & Technology Review*, vol. 30, no. 15, pp. 61–74, 2012.

[4] L. C. Ji, "Review and prospect on research of counter-rotating turbine," *Aeroengine*, vol. 4, pp. 49–53, 2006.

[5] S. Y. Liu, P. Wang, X. J. Fang, and S. P. Yan, "Research on aerodynamic design of counter-rotating turbine without

intermediate vanes," *Gas Turbine Experiment and Research*, vol. 1, pp. 20–37, 2002.

[6] P. Bellocq, I. Garmendia, J. Legrand, and V. Sethi, "Preliminary design and performance of counter rotating turbines for open rotors: part I—1-D methodology," in *Proceedings of the ASME Turbo Expo 2016: Turbomachinery Technical Conference and Exposition. Volume 1: Aircraft Engine; Fans and Blowers; Marine*, Seoul, South Korea, 2016.

[7] P. Bellocq, I. Garmendia, J. Legrand, and V. Sethi, "Preliminary design and performance of counter rotating turbines for open rotors: part II — 0-D methodology and case study for a 160 PAX aircraft," in *Proceedings of the ASME Turbo Expo 2016: Turbomachinery Technical Conference and Exposition. Volume 1: Aircraft Engine; Fans and Blowers; Marine*, Seoul, South Korea, 2016.

[8] W. T. Wintucky and W. L. Stewart, "Analysis of two-stage counterrotating turbine efficiencies in terms of work and speed requirements," National Advisory Committee for Aeronautics, 1958.

[9] B. A. Ponomariov, "New generation of the small turboshaft and turboprop engines in the U.S.S.R," in *Proceedings of the ASME 1990 International Gas Turbine and Aeroengine Congress and Exposition. Volume 2: Aircraft Engine; Marine; Microturbines and Small Turbomachinery*, Brussels, Belgium, 1990.

[10] B. A. Ponomariov and Y. V. Sotsenko, "Using contra-rotating rotors for decreasing sizes and component number in small GTE," in *Proceedings of the ASME 1992 International Gas Turbine and Aeroengine Congress and Exposition. Volume 2: Aircraft Engine; Marine; Microturbines and Small Turbomachinery*, Cologne, Germany, 1992.

[11] Y. V. Sotsenko, "Thermogasdynamic effects of the engine turbines with the contra-rotating rotors," in *Proceedings of the ASME 1990 International Gas Turbine and Aeroengine Congress and Exposition. Volume 1: Turbomachinery*, Brussels, Belgium, 1990.

[12] A. Yamamoto, "Recent fundamental research on turbine steady and unsteady aerodynamics at the National Aerospace Laboratory in Japan," in *Turbomachinery Fluid Dynamics and Heat Transfer*, pp. 383–403, 2017.

[13] A. Yamamoto and E. Outa, "Low-speed annular cascade tests of an ultra-highly loaded turbine with tip clearance, part 1-near design incidence," in *ASME 1999 International Gas Turbine and Aeroengine Congress and Exhibition*, Indianapolis, Indiana, USA, 1999.

[14] F. Huber, B. Branstrom, A. Finke, P. Johnson, R. Rowey, and J. Veres, "Design and test of a small two stage counter-rotating turbine for rocket engine application," in *29th Joint Propulsion Conference and Exhibit*, Monterey, CA, U.S.A, 1993.

[15] C. W. Haldeman, M. G. Dunn, R. S. Abhari, P. D. Johnson, and X. A. Montesdeoca, "Experimental and computational investigation of the time-averaged and time-resolved pressure loading on a vaneless counter-rotating turbine," in *Proceedings of the ASME Turbo Expo 2000: Power for Land, Sea, and Air. Volume 1: Aircraft Engine; Marine; Turbomachinery; Microturbines and Small Turbomachinery*, Munich, Germany, 2000.

[16] B. D. Keith, D. K. Basu, and C. Stevens, "Aerodynamic test results of controlled pressure ratio engine (COPE) dual spool air turbine rotating rig," in *proceedings of the asme turbo Expo 2000: Power for Land, Sea, and Air. Volume 1: Aircraft Engine; Marine; Turbomachinery; Microturbines and Small Turbomachinery*, Munich, Germany, 2000.

[17] Z. Wu, X. Fang, S. Liu, and D. Zhao, "Experimental research of 1 + 3/2 contra-rotating turbine aerodynamic performance," *Journal of Beijing University of Aeronautics and Astronautics*, vol. 42, no. 12, pp. 2676–2682, 2016.

[18] W. Zhongye, F. Xiangjun, L. Siyong, and M. Guangjian, "Test and analysis on aerodynamic performance of 1+1/2 super-transonic counter-rotating turbine," *Acta Aeronautica et Astronautica Sinica*, vol. 39, no. 9, pp. 122155–122164, 2018.

[19] H. S. Wang, H. She, Q. J. Zhao et al., "Numerical study on tip clearance flow field of 1+1/2 counter rotating turbine high pressure blade," *Journal of Engineering Thermophysics*, vol. 5, pp. 751–754, 2007.

[20] H. Wang, Q. Zhao, X. Zhao, and J. Xu, "Unsteady numerical simulation of shock systems in vaneless counter-rotating turbine," in *Proceedings of the ASME Turbo Expo 2005: Power for Land, Sea, and Air. Volume 6: Turbo Expo 2005, Parts A and B. Reno*, Nevada, USA, 2005.

[21] Q. J. Zhao, H. S. Wang, X. L. Zhao, and J. Z. Xu, "Unsteady numerical simulation of three-dimensional flow field in counter rotating turbine without guide vanes," *Journal of Engineering Thermophysics*, vol. 1, pp. 35–38, 2006.

[22] Y. M. Zhao and R. D. Sandberg, "High-fidelity simulations of a high-pressure turbine vane subject to large disturbances: effect of exit Mach number on losses," *Journal of Turbomachinery*, vol. 143, no. 9, 2021.

[23] J. Sousa, E. Collado-Morata, and G. Paniagua, "Design and optimization of supersonic turbines for detonation combustors," *Chinese Journal of Aeronautics*, vol. 35, no. 11, pp. 33–44, 2022.

[24] NUMECA International, *User Manual FINE/Turbo v8 - Flow Integrated Environment*, NUMECA International, 2007.